

Letter

Benzothiadiazole Based Cascade Material to Boost the Performance of Inverted Ternary Organic Solar Cells

Miron Krassas ^{1,2,†}, Christos Polyzoidis ^{1,†}, Pavlos Tzourmpakis ¹, Dimitrios M. Kosmidis ¹ , George Viskadourous ^{1,3} , Nikolaos Kornilios ¹, George Charalambidis ⁴ , Vasilis Nikolaou ⁴ , Athanassios G. Coutsolelos ⁴ , Konstantinos Petridis ^{5,*}, Minas M. Stylianakis ^{1,*}  and Emmanuel Kymakis ^{1,*} 

¹ Department of Electrical & Computer Engineering, Hellenic Mediterranean University, 71410 Heraklion, Crete, Greece; kmiron@hmu.gr (M.K.); polyzoidis@hmu.gr (C.P.); ptzourmpakis@gmail.com (P.T.); kosdimitris@hmu.gr (D.M.K.); viskadourous@hmu.gr (G.V.); kornil@hmu.gr (N.K.)

² Department of Materials Science and Technology, University of Crete, 71003 Heraklion, Crete, Greece

³ Department of Mineral Resources Engineering, Technical University of Crete, 73100 Chania, Crete, Greece

⁴ Laboratory of Bioinorganic Chemistry, Chemistry Department, University of Crete, Voutes Campus, 71003 Heraklion, Crete, Greece; gxaral@chemistry.uoc.gr (G.C.); v.nikolaou@uoc.gr (V.N.); coutsole@chemistry.uoc.gr (A.G.C.)

⁵ Department of Electronic Engineering, Hellenic Mediterranean University, 73132 Chania, Crete, Greece

* Correspondence: c.petridischania@gmail.com (K.P.); stylianakis@hmu.gr (M.M.S.); kymakis@hmu.gr (E.K.); Tel.: +30-2810-379775 (M.M.S.)

† These authors contributed equally to this work.

Received: 10 November 2019; Accepted: 15 January 2020; Published: 17 January 2020



Abstract: A conjugated, ladder-type multi-fused ring 4,7-dithienbenzothiadiazole:thiophene derivative, named as compound 'T', was for the first time incorporated, within the PTB7:PC₇₁BM photoactive layer for inverted ternary organic solar cells (TOSCs) realization. The effective energy level offset caused by compound T between the polymeric donor and fullerene acceptor materials, as well as its resulting potential as electron cascade material contribute to an enhanced exciton dissociation, electron transfer facilitator and thus improved overall photovoltaic performance. The engineering optimization of the inverted TOSC, ITO/PFN/PTB7:Compound T(5% v/v):PC₇₁BM/MoO₃/Al, resulted in an overall power conversion efficiency (PCE) of 8.34%, with a short-circuit current density (J_{sc}) of 16.75 mA cm⁻², open-circuit voltage (V_{oc}) of 0.74 V and a fill factor (FF) of 68.1%, under AM1.5G illumination. This photovoltaic performance was improved by approximately 12% with respect to the control binary device.

Keywords: organic solar cells; ternary blend; bulk heterojunction; cascade effect; charge transfer; additive; benzothiadiazole; small molecule

1. Introduction

The prevalent research rush of the scientific community towards cost-effective and reliable alternative energy sources involves the whole spectrum of research on photovoltaic technologies and corresponding material science. Recent progress in the subfield of organic solar cells (OSCs) highlights and even updates their potential as ideal, low-cost alternatives to the conventional inorganic silicon technology. This is attributed to their advantages, such as light-weight and solution-processability, as well as their compatibility with flexible substrates and upscaling techniques [1–3]. The emergence of novel materials [4–7], advancements of device's engineering [1,8,9] for enhanced light harvesting and trapping by extending the absorption spectrum or introducing optical cavities [10,11], and additionally leading theoretical studies [12,13], have so far skyrocketed their efficiency over 13% [8].

Solution-processed bulk-heterojunction (BHJ) photovoltaics constitute a subcategory of OSCs that already enjoys immense research. The careful selection of polymer donor and fullerene acceptor materials, having in mind the proper energy level matching and appropriate degree of phase separation inside the blend, has introduced additional degrees of freedom into OSC research and scientific advancement [14–16]. Polymers, including P3HT [17] and PTB7 [18], as well as fullerene derivatives with most notable PC₆₁BM [19] and PC₇₁BM [20] have been under study for years while demonstrating exceptional efficiencies (>5%) for P3HT:PC₆₁BM [21] and above 7% for PTB7:PC₇₁BM based devices [22]. On the other hand, a very promising subfield of OSC research employs non-fullerene acceptors (NFAs) that yield state-of-the-art OSC cells with impressive efficiencies exceeding 16% [23–25]. However, NFA based OSCs remain partially explored and extensive optimization efforts are required, in order to counter the competitive advantages of conventional fullerene-based materials. For instance, PC₇₁BM-based active blends result to OSCs that yield better photostability under operational conditions [26–28]. On top of that, tailor-made polymer fabrication is an additional way of research towards efficient OSCs. Many polymers have been prepared through alternating copolymerization of donor (D) and electron acceptor (A) units, thereby resulting in D–A pairs that effectively (a) exhibit multiple and complementary absorptions; and (b) enhance charge transfer ability [4].

Another effective, yet simple strategy to enhance the OSC's photovoltaic performance is the adoption of a ternary structure into a binary system. This can be secured with the integration into the active layer of a third component [29–32]. This third element could be a polymer [32–35], an organic small molecule [36–49], a dye [50–52], a fullerene derivative [53], a graphene and a two dimensional (2D)-based material [54–59], or a nanocrystal [60]. The introduction and the availability of materials to be leveraged as third element support the better engineering of this architecture towards better photovoltaic OSCs' performances. The third component within ternary organic solar cells (TOSCs) may function as a charge relay for electron and hole transport [56,58], as an energy transfer step, act as a second donor [61], as well as create a new organic blend with new physical characteristics in conjunction with the donor. In the cases where the charge transfer mechanism prevails, the third component needs to be placed at the interface of the host donor and the acceptor in order, efficient charge transfer to take place; the so-called energy level "cascade" phenomenon [29,57]. Careful design and selection of the third component, as a function of its energy levels, electrical conductivity, electron mobility and chemical properties, necessitate to ensure efficient charge transfer through the active layer of TOSC [62]. The careful selection and introduction of the third element impacts the photovoltaic properties of the resulting solar cell such as optical properties, the extension of the absorption's bandwidth and intensity, the improved charge or energy transfer efficiency, by regulating the local environment at the D:A interfaces, thereby securing a better exciton generation and dissociation [36,37]. As a consequence, an improvement in efficiency may end up to power conversion efficiency (PCE) values of the order of 8–10% [33,37,63].

2,1,3-Benzothiadiazole (BT), an electron-deficient unit, is among the most common building blocks utilized for the lowering of potential and electron affinity of electron-transport materials [64,65]. BT is a n-type building block consisting of a benzene ring fused to one of thiadiazole [66,67], that can be coupled with an electronically rich molecule to form low bandgap functional polymers or small molecules [68]. Moreover, the cyano groups bound to the benzene ring can operate as electron scavenging units. Following this recipe, the lowest unoccupied molecular orbital (LUMO) level of the polymer can be reportedly lowered due to the benzene ring in an effective way [69].

In this work, a ladder-type vinyl complex based on cyanovinylene bonds, 4,7-dithien-benzothiadiazole as central unit and thiophene rings as terminal units, was synthesized and characterized in terms of its photophysical and electrochemical properties. The synthesized conjugated small molecule (CSM), named compound T [70], was integrated as the third component, into a binary BHJ PTB7:PC₇₁BM active layer in different concentrations (3–15%) ratio to the polymeric donor. Upon the incorporation of compound T in 5% as optimum determined concentration, a PCE of 8.34% was achieved for the champion inverted TOSC device, improved by 12% with respect to the control inverted binary device.

2. Materials and Methods

2.1. Materials and Instruments

PTB7 was purchased from Solaris Chem, while PC₇₁BM and PFN were both purchased from Solenne BV. CSM was synthesized according to a multi-step procedure, successively containing donor–acceptor moieties seriatim. More specifically, two phenyl or thiophene rings were linked to the 4,7-dithienbenzothiadiazole core unit, through a cyano-substituted vinylene bond. The chemical structures of PTB7, compound T and PC₇₁BM, employed in the ternary BHJ, are illustrated in Figure 1. Such an approach is popular and is widely utilized to reduce the band gap of conjugated semiconductors [71,72]. The exact synthetic procedure of compound T can be found in another publication of our research team and is analyzed in Figure S1 [70].

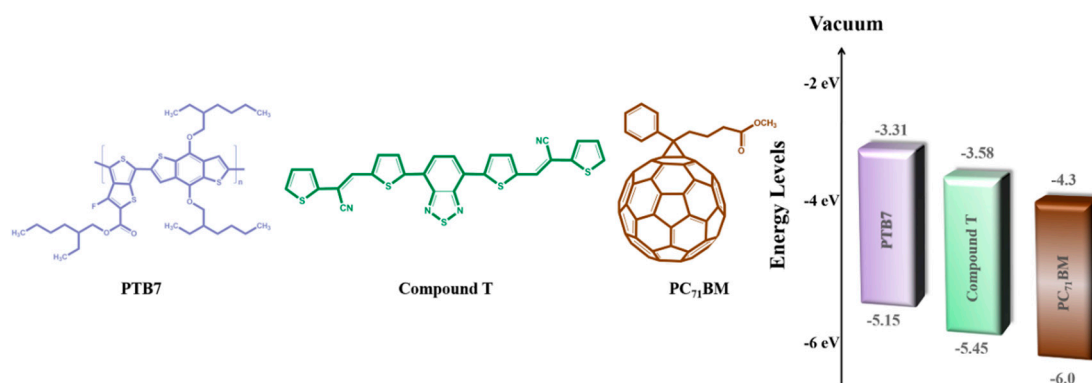


Figure 1. Chemical structures and energy levels of ternary blend's component.

UV-vis absorption spectra were taken using a Shimadzu UV-2401 PC spectrophotometer to a wavelength range of 300–800 nm. The photoluminescence (PL) spectra of the ternary active layers were conducted at room temperature (RT) and set through a UV sensitive, calibrated CCD camera, liquid N₂ cooled—over a wavelength range of 600–950 nm. The excitation source employed was a He–Cd CW laser at 325 nm with a full power of $P_0 = 35$ mW. The morphologies of the surfaces were examined with an atomic force microscope (Park Systems XE7). The OSC device photovoltaic parameters (J_{sc} , V_{oc} , FF and PCE) were measured at room temperature within glove box (MBRAUN) conditions ($O_2 < 0.1$ ppm), moisture-free ($H_2O < 0.1$ ppm) and under standard illumination conditions (at AM 1.5 G and an intensity of 1000 Wm^{-2}). The external quantum efficiency (EQE) curves of the devices were extracted under short-circuit conditions immediately, in order to avoid any device degradation, using an integrated system (Enlitech, Taiwan) equipped with a lock-in amplifier with a current preamplifier. To further enhance the credibility of our measurements, a monocrystalline photodetector of known spectral response was used to calibrate the spectrum of the solar simulator. OSC devices were assessed using a xenon (Xe) lamp, as well as an optical chopper at low frequencies (200 Hz) in order to get the maximum signal/noise (S/N) ratio. To ensure the reproducibility of the J – V characteristics, ten same devices consisting of six photovoltaics cells each were fabricated and evaluated.

2.2. Device Fabrication

A conventional procedure was followed for OSC devices fabrication [16]. More specifically, OSCs were fabricated onto glass substrates sputtered with indium-tin-oxide (ITO) that exhibited a $20 \Omega \text{ sq}^{-1}$ sheet resistance. To remove any impurities from the ITO glass, ultrasonic bath (Elma S 30 H Elmasonic) for 10 min was applied using three different washing components, namely Hellmanex III detergent, acetone and isopropanol in subsecutive steps, and then dried in an oven. Finally, a UV-ozone treatment was performed for 15 min. The inverted structure was preferred for fabricating the OSC devices.

PFN solution, with concentration 0.5 mg/mL, was dispersed in 1 mL of methanol (MeOH) and 2 μ L of acetic acid and was stirred overnight. Then PFN layer (ETL) was spin-cast at 1000 rpm for 45 s but, in order to achieve layer thickness of approximately 10 nm, a multilayer approach was used. Specifically, four layers of PFN solution were developed with intermittent annealing steps at 150 $^{\circ}$ C for 30 s between each spin-coating stage. PTB7 and PC₇₁BM, were blended (25 mg/mL, ratio 1:1.5) in chlorobenzene (CB):DIO (97:3 vol%) solvents' mixture. The said photoactive layer was subsequently developed by spin-coating of the blend solutions at 1500 rpm on top of the PFN layer with a thickness of 85 nm. Thereafter, a MoO₃ layer (8 nm) and the Al electrode (100 nm) were thermally evaporated through a shadow mask hence defining an active area of 4 mm² for each device.

3. Results and Discussion

3.1. Photophysical Properties

Compound T was characterized using UV-vis, FT-IR and PL spectroscopy. The UV-vis absorption spectrum of a thin film pristine compound T exhibited two main peaks at 398 nm and 485 nm, respectively (Figure 2), which were both due to the $\pi \rightarrow \pi^*$ electron transition.

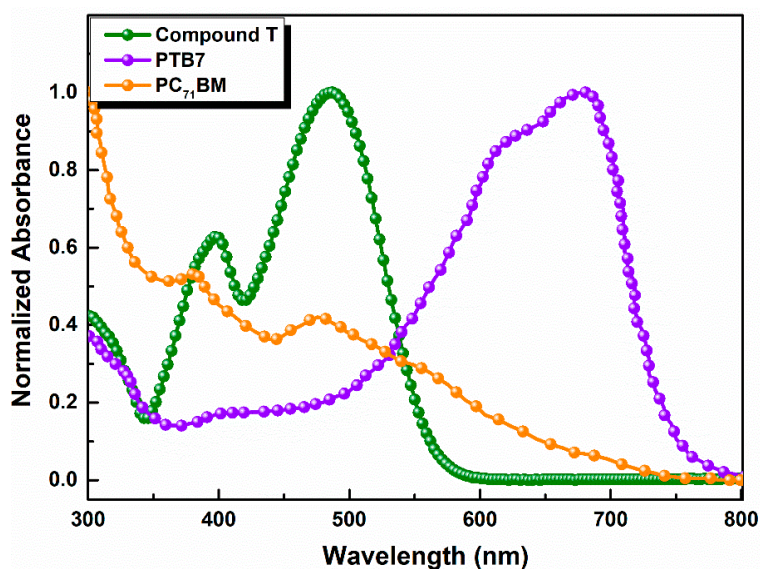


Figure 2. Normalized UV-Visible absorption spectra of Compound, PTB7 and PC₇₁BM in thin films.

According to the FT-IR spectrum of compound T [70] (Figure S2) a characteristic peak at 2214 cm^{-1} appears, due to the CN-stretching bond. The peak at 3103 cm^{-1} is ascribed to aromatic C–H stretching, while the absorption bands at 1652 cm^{-1} , 1577 cm^{-1} , 1533 cm^{-1} , 1520 cm^{-1} , 1479 cm^{-1} and 1441 cm^{-1} correspond to C=C aromatic stretching bonds, respectively. Finally, peaks at 1267 cm^{-1} , 1252 cm^{-1} , 1243 cm^{-1} , 1224 cm^{-1} , 1203 cm^{-1} , 1189 cm^{-1} , 1097 cm^{-1} , 1080 cm^{-1} and 1048 cm^{-1} are attributed to the benzene ring of benzothiazole. On the other hand, the PL spectrum of compound T in solid state was recorded in the range of 600–900 nm, upon photoexcitation at 485 nm, as depicted in Figure S3. Compound T exhibited a broad peak at 700 nm.

In Figure 3 the absorption spectra of the ternary active layers are illustrated. It is observable that the absorption intensity slightly increased as the concentration of compound T got 5% across the full spectrum range and especially between 400 and 560 nm, where the host PTB7 and compound T spectra overlapped. Moreover, the common peak of compound T and fullerene derivative PC₇₁BM got higher values, while the absorption peak of PTB7, decreased. According to relevant existing literature [73], two broad absorption peaks at around 614 and 682 nm are attributed to the characteristic $\pi\text{-}\pi^*$ transition of the PTB7 polymer.

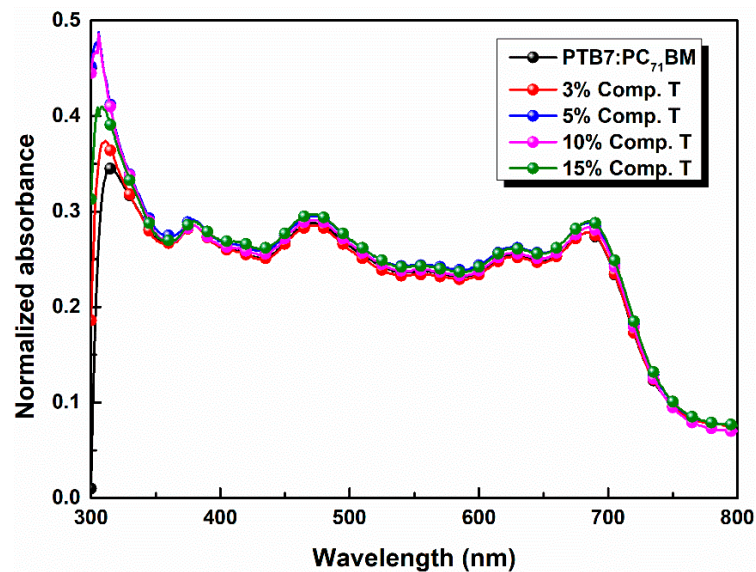


Figure 3. Normalized UV-vis absorption spectra of PTB7:PC₇₁BM blends incorporating compound T in different concentrations.

In the latter, the photoluminescence (PL) spectrum of PTB7:compound T was quenched as an optimum concentration value of the third element was approaching its optimum value. The PL quenching is clear evidence of the improved exciton dissociation, between compound T and PTB7, as the emission of the latter quenched (Figure 4). The best charge extraction was observed after the addition of 5% v/v Compound T, compared to the reference binary system (PTB7:PC₇₁BM). This is a possible reason for the enhanced PV parameters in the case of 3% and 5% ternary devices, as demonstrated below in Table 1. This fact proves that compound T could act as an electron cascade material that facilitates the higher electron extraction from PTB7 towards PC₇₁BM compared to the binary reference system.

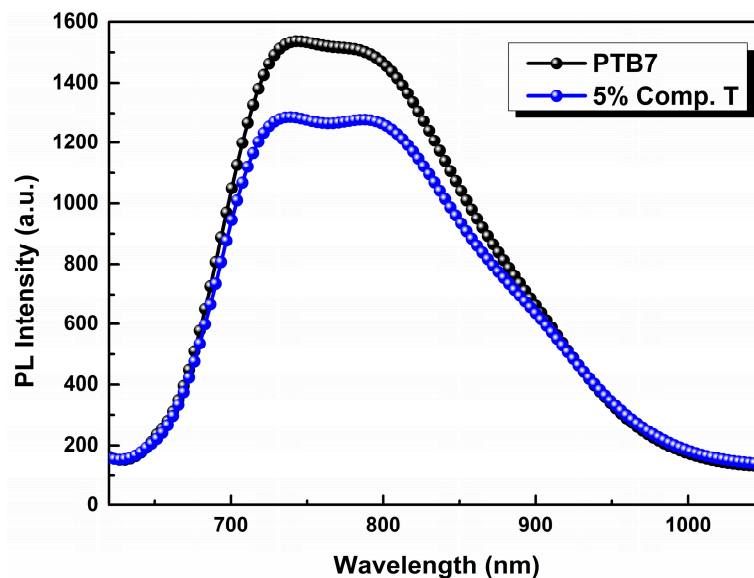


Figure 4. Photoluminescence (PL) spectra of PTB7 (black) and PTB7:compound T (5%; blue) thin film on a Si substrate.

3.2. Photovoltaic Performance

A schematic representation of the inverted ternary OSC structured as ITO/PFN/PTB7:compound T:PC₇₁BM/MoO₃/Al is depicted in Figure 5, while the respective configuration and energy diagram of

the device with the HOMO and LUMO energy levels of the materials selected are depicted in Figure 1. Due to the energy level offset between PTB7 [74], compound T [70] and PC₇₁BM [74] (3.31 eV, 3.58 eV and 4.3 eV in LUMO level and 5.15 eV, 5.48 eV and 6.0 eV in the HOMO level, respectively) the charge transfer is enhanced. This is clear evidence, that the addition of compound T up to an optimum concentration, promoted the electron-cascade effect. More specifically, excitons are dissociated at the D:A interfaces throughout the blend layer. Since the HOMO levels of compound T and the conjugated polymer PTB7 perfect match, holes' transport was facilitated through the compound T en route to the anode electrode. In Figure 5, current-to-voltage characteristics based on the PTB7:PC₇₁BM and the ternary PTB7:compound T:PC₇₁BM active layers, are also depicted. The corresponding PV performance parameters are listed in Table 1. The reference binary device exhibited a short circuit current density (J_{sc}) of 16.10 mA cm⁻², an open circuit voltage (V_{oc}) at 0.72 V, a fill factor (FF) at 64.6% and a PCE of 7.51%.

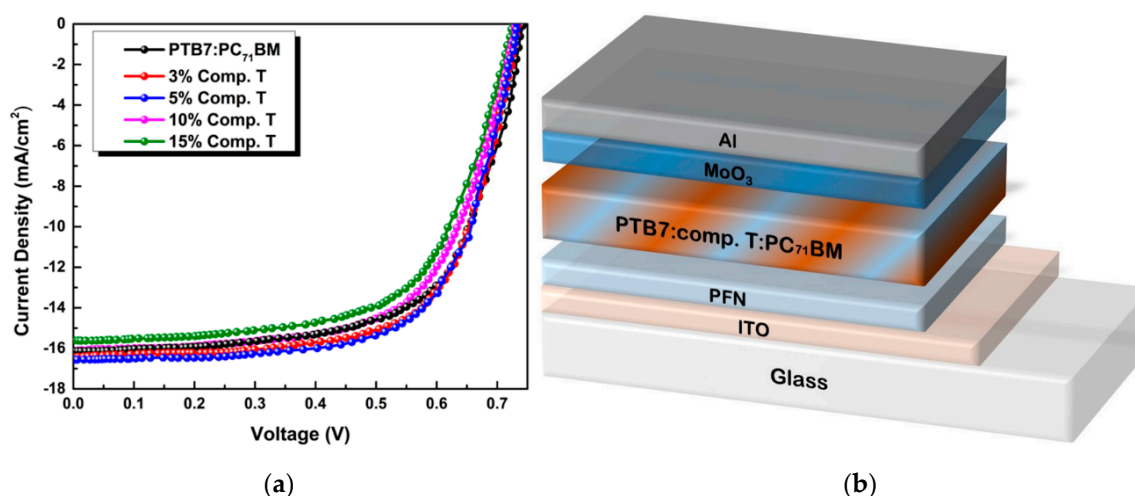


Figure 5. Current density to voltage characteristics of different concentrations of compound T in PTB7:PC₇₁BM blend (a) and a schematic representation of the ternary bulk heterojunction device structure (b).

As shown, J_{sc} did not follow the rising trend of compound T concentration, but instead it increased from 3% to 5% and then started to decay as the concentration of compound T got higher values. This was attributed to the degradation of the interfaces between compound T and the polymer donor material. On the other hand, the V_{oc} obtained in the ternary cells was almost identical to the binary PTB7:PC₇₁BM, reflecting that charge transfer state energy (E_{CT}) does not change upon the addition of Compound T [75].

Table 1. Summary of solar cell parameters of PTB7:PC₇₁BM and ternary PTB7:compound T:PC₇₁BM blend with different concentrations *.

Concentration of Compound T	Calc. J_{sc} (mA cm ⁻²)	J_{sc} (mA cm ⁻²)	V_{oc} (V)	FF (%)	PCE (%)
Reference	15.62	16.10 ± 0.08	0.72 ± 0.04	64.6 ± 0.6	7.51 ± 0.12
3% v/v	16.00	16.44 ± 0.11	0.73 ± 0.02	65.9 ± 0.3	7.96 ± 0.11
5% v/v	16.20	16.70 ± 0.05	0.73 ± 0.01	67.7 ± 0.4	8.25 ± 0.09
10% v/v	15.58	16.06 ± 0.11	0.73 ± 0.02	64.0 ± 0.3	7.50 ± 0.11
15% v/v	15.14	15.61 ± 0.13	0.72 ± 0.01	63.3 ± 0.1	7.11 ± 0.09

* The data were averaged from ten identical organic solar cell (OSC) devices with six cells each.

3.3. Charge Transfer Properties

In view of further investigating the origin of the J_{sc} increase upon the addition of the compound T up to an optimum concentration, the incident photon to electron conversion efficiency was measured (IPCE) for each device (Figure 6). From EQE curves, it was deduced that the 5% concentration (v/v) had the best response at both main absorption peaks, which indicates that this ratio might yield the most efficient charge transportation and collection due to a better domain engineering within the active layer of the ternary system.

Carriers' mobilities of the reference device (PTB7:PC₇₁BM) and the ternary one, incorporating 5% compound T, were also obtained by space charge limited current (SCLC) method. To this end, hole and electron only devices of the structure ITO/PEDOT:PSS/active layer/MoO₃/Au and ITO/PFN/active layer/Ca/Al were respectively fabricated and J - V^2 characteristic curves are reported (Figure S5). Calculations were based on the Mott–Gurney equation [76]:

$$J_{SCLC} = \frac{9}{8} \varepsilon_r \varepsilon_0 \mu \frac{(V - V_{bi})^2}{d^3}, \quad (1)$$

where ε_r is the relative dielectric constant, ε_0 is the permittivity of free space, μ is the charge carrier mobility, V is the applied voltage, V_{bi} is the built-in potential and d is the thickness of the active layer.

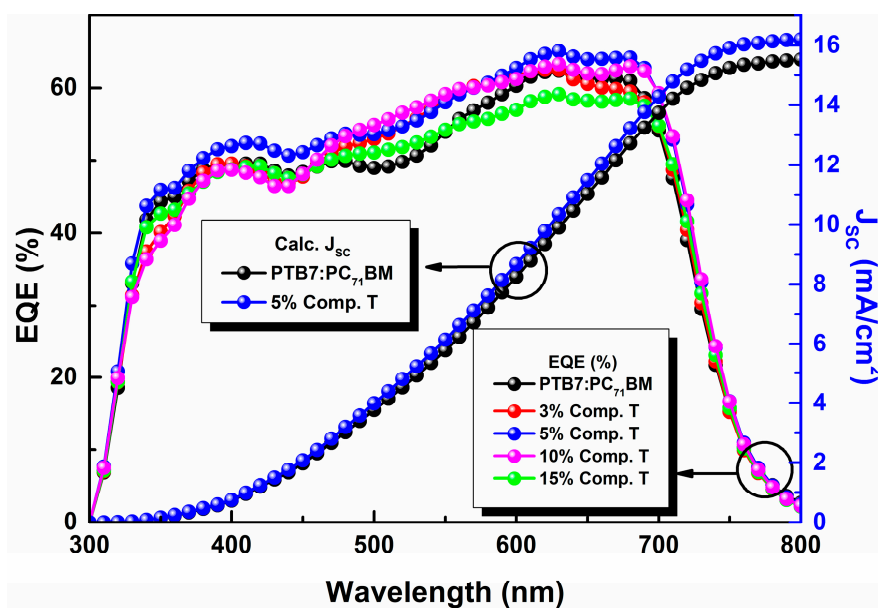


Figure 6. External quantum efficiency (EQE) curves of the reference (black), 3% (red), 5% (blue), 10% (violet) and 15% (green) compound T based OSC devices.

The μ_h and μ_e values for holes and electrons mobilities of the reference and 5% compound T ternary device are summarized in Table 2, respectively. It is obvious that the incorporation of compound T into the binary solution resulted to the improvement of hole mobility, an even higher increase in electron mobility and most important the more balanced ratio between hole and electron mobilities. Moreover, the fact that the μ_h/μ_e ratio is closer to one for the case of the ternary device, is a key prerequisite in avoiding charge accumulation in the device and thus higher photovoltaic performances. The aforementioned result confirms the previous assumption for the electron-cascade-role of compound T.

Table 2. Hole and electron mobilities of PTB7:PC₇₁BM and ternary blend PTB7:compound T (5%):PC₇₁BM *.

Active Layer	μ_h (cm ² ·V ⁻¹ ·s ⁻¹)	μ_e (cm ² ·V ⁻¹ ·s ⁻¹)	Ratio (μ_h/μ_e)
PTB7:PC ₇₁ BM (reference)	9.91×10^{-5}	8.01×10^{-5}	1.24
5% compound T	1.01×10^{-4}	8.61×10^{-5}	1.17

* The data were averaged from ten identical OSC devices with six cells each.

3.4. Morphology

In order to study the effect of compound T on active layer's morphology, a reference and a ternary blend layer of 5% (v/v) concentration were subjected to AFM measurements. Subsequent results (Figure S4) indicate a better morphology together with a reduction in roughness (RMS) for the ternary device containing 5% of compound T, by approximately 9.1%. In particular, the RMS value for the reference binary layer was 1.4 nm, whereas the ternary layer demonstrated an RMS value of approximately 1.28 nm. This is proof that the addition of compound T enhances the interface quality between the active layer and hole transport layer, thereby indicating an improvement in FF and other PV parameters [77].

4. Conclusions

In conclusion, simple ternary inverted organic solar cells incorporating the soluble compound T, into the photoactive layer of the binary PTB7:PC₇₁BM blend were fabricated by differentiating additive's concentration from 3% to 15%. The incorporation of the compound T led to a favorable energy alignment between the energy levels of PTB7 donor and PC₇₁BM acceptor, thus facilitating the electron-cascade effect. The champion ternary blend device based on the ITO/PFN/PTB7:compound T:PC₇₁BM/MoO₃/Al structure, with a 5% (v/v) concentration of compound T, resulted in a PCE of 8.34%, with an enhancement of 12% compared to the reference device. Therefore, since compound T had a wide optical bandgap and low HOMO level, it demonstrated the potential for boosting device performance of other visible, as well as the near-infrared non-fullerene blends like, which are of great interest for the OSC community.

Supplementary Materials: The synthetic procedure of compound T and its intermediate stages, as well as explanations of experimental details to understanding and reproducing the research are available online at <http://www.mdpi.com/1996-1073/13/2/450/s1>, Figure S1: Five-step synthesis of compound T, Figure S2: FT-IR spectrum of compound T, Figure S3: Normalized PL spectrum of compound T in thin film, Figure S4: AFM images of (a) binary and (b) ternary bulk heterojunction film with 5% compound T content, Figure S5: $J-V^2$ characteristics of the fabricated (a) electron-only and (b) hole-only devices, upon the addition of 5% compound T, for the determination of carriers' mobilities.

Author Contributions: Conceptualization, P.T. and M.M.S.; Methodology, M.K., C.P., P.T., D.M.K., K.P. and M.M.S.; Formal Analysis, M.K., G.V. and M.M.S.; Investigation, M.K., P.T. and M.M.S.; Data Curation, M.K., P.T., G.V., N.K., G.C., V.N. and M.M.S.; Writing—Original Draft Preparation, M.K., C.P., P.T. and M.M.S.; Writing—Review and Editing, A.G.C., K.P. and M.M.S.; Supervision, M.M.S. and E.K.; Project Administration, K.P. and M.M.S. Funding Acquisition, K.P. and M.M.S. All authors have read and agreed to the published version of the manuscript.

Funding: This research was co-funded by the Erasmus Plus Capacity Building Project entitled "Innovative Photonic Education in Nanotechnology—iPEN" of the European Union with project number 586165-EPP-1-2017-1-EL-EPPKA2-CBHE-JP.

Conflicts of Interest: The authors declare no conflict of interest.

References

1. Cao, W.; Xue, J. Recent progress in organic photovoltaics: Device architecture and optical design. *Energy Environ. Sci.* **2014**, *7*, 2123–2144. [CrossRef]
2. Li, Y.F. Molecular design of photovoltaic materials for polymer solar cells: Toward suitable electronic energy levels and broad absorption. *Acc. Chem. Res.* **2012**, *45*, 723–733. [CrossRef] [PubMed]

3. Li, G.; Zhu, R.; Yang, Y. Polymer solar cells. *Nat. Photon.* **2012**, *6*, 153–161. [[CrossRef](#)]
4. Mikroyannidis, J.A.; Stylianakis, M.M.; Sharma, G.D.; Balraju, P.; Roy, M.S. A novel alternating phenylenevinylene copolymer with perylene bisimide units: Synthesis, photophysical, electrochemical, and photovoltaic properties. *J. Phys. Chem. C* **2009**, *113*, 7904–7912. [[CrossRef](#)]
5. Lu, L.; Yu, L. Understanding low bandgap polymer PTB7 and optimizing polymer solar cells based on it. *Adv. Mater.* **2014**, *26*, 4413–4430. [[CrossRef](#)]
6. Mikroyannidis, J.A.; Stylianakis, M.M.; Suresh, P.; Roy, M.S.; Sharma, G.D. Synthesis of perylene monoimide derivative and its use for quasi-solid-state dye-sensitized solar cells based on bare and modified nano-crystalline ZnO photoelectrodes. *Energy Environ. Sci.* **2009**, *2*, 1293–1301. [[CrossRef](#)]
7. Sharma, G.D.; Suresh, P.; Mikroyannidis, J.A.; Stylianakis, M.M. Efficient bulk heterojunction devices based on phenylenevinylene small molecule and perylene-pyrene bisimide. *J. Mater. Chem.* **2010**, *20*, 561–567. [[CrossRef](#)]
8. Zhang, S.; Ye, L.; Hou, J. Breaking the 10% efficiency barrier in organic photovoltaics: Morphology and device optimization of well-known PBDTTT polymers. *Adv. Energy Mater.* **2016**, *6*, 1502529. [[CrossRef](#)]
9. Guo, X.; Zhou, N.; Lou, S.J.; Smith, J.; Tice, D.B.; Hennek, W. Polymer solar cells with enhanced fill factors. *Nat. Photon.* **2013**, *7*, 825–833. [[CrossRef](#)]
10. Liu, Q.; Toudert, J.; Li, T.; Kramarenko, M.; Martínez-Denegri, G.; Ciammaruchi, L.; Zhan, X.; Martorell, J. Inverse optical cavity design for ultrabroadband light absorption beyond the conventional limit in low-bandgap nonfullerene acceptor-based solar cells. *Adv. Energy Mater.* **2019**, *9*, 1900463. [[CrossRef](#)]
11. Liu, Q.; Romero-Gomez, P.; Mantilla-Perez, P.; Colodrero, S.; Toudert, J.; Martorell, J. A two-resonance tapping cavity for an optimal light trapping in thin-film solar cells. *Adv. Energy Mater.* **2017**, *7*, 1700356. [[CrossRef](#)]
12. Kakavelakis, G.; Vangelidis, I.; Jungemann, H.; Kanaras, A.G.; Lidorikis, E.; Stratakis, E.; Kymakis, E. Photovoltaic devices: Plasmonic backscattering effect in high-efficient organic photovoltaic devices. *Adv. Energy Mater.* **2015**, *6*, 1501640. [[CrossRef](#)]
13. Noori, K.; Konios, D.; Stylianakis, M.M.; Kymakis, E.; Giustino, F. Energy-level alignment and open-circuit voltage at graphene/polymer interfaces: Theory and experiment. *2D Mater.* **2016**, *3*, 015003. [[CrossRef](#)]
14. Tiwari, S.; Tiwari, T.; Carter, S.; Scott, J.; Yakhmi, J. Advances in polymer-based photovoltaic cells: Review of pioneering materials, design, and device physics. In *Handbook of Ecomaterials*, 1st ed.; Martínez, L., Kharissova, O., Kharisov, B., Eds.; Springer: Cham, Switzerland, 2019; pp. 1055–1101.
15. Huang, W.; Cheng, P.; Yang, Y.; Li, G.; Yang, Y. High-performance organic bulk-heterojunction solar cells based on multiple-donor or multiple-acceptor components. *Adv. Mater.* **2018**, *30*, 1705706. [[CrossRef](#)]
16. Anagnostou, K.; Stylianakis, M.M.; Petridis, K.; Kymakis, E. Building an organic solar cell: Fundamental procedures for device fabrication. *Energies* **2019**, *12*, 2188. [[CrossRef](#)]
17. Marrocchi, A.; Lanari, D.; Facchetti, A.; Vaccaro, L. Poly(3-hexylthiophene): Synthetic methodologies and properties in bulk heterojunction solar cells. *Energy Environ. Sci.* **2012**, *5*, 8457–8474. [[CrossRef](#)]
18. Liang, Y.; Feng, D.; Wu, Y.; Tsai, S.T.; Li, G.; Ray, C.; Yu, L. Highly efficient solar cell polymers developed via fine-tuning of structural and electronic properties. *J. Am. Chem. Soc.* **2009**, *131*, 7792–7799. [[CrossRef](#)] [[PubMed](#)]
19. Matsumoto, F.; Moriwaki, K.; Takao, Y.; Ohno, T. Synthesis of thienyl analogues of PCBM and investigation of morphology of mixtures in P3HT. *Beilstein J. Org. Chem.* **2008**, *4*, 33. [[CrossRef](#)]
20. Li, C.Z.; Yip, H.L.; Jen, A.K.Y. Functional fullerenes for organic photovoltaics. *J. Mater. Chem.* **2012**, *22*, 4161–4177. [[CrossRef](#)]
21. Berger, P.; Kim, R.; Kim, M. Polymer solar cells: P3HT: PCBM and beyond. *J. Renew. Sustain. Energy* **2018**, *10*, 013508. [[CrossRef](#)]
22. Chen, C.P.; Lee, I.; Tsai, C.; Huang, Y.; Chen, C.L.; Huang, G.W. Efficient organic solar cells based on PTB7:PC₇₁BM blend film with embedded different shapes silver nanoparticles into PEDOT: PSS as hole transporting layers. *Org. Electron.* **2018**, *62*, 95–101. [[CrossRef](#)]
23. Cui, Y.; Yao, H.; Hong, L.; Zhang, T.; Tang, Y.; Lin, B.; Xian, K.; Gao, B.; An, C.; Bi, P.; et al. 17% efficiency organic photovoltaic cell with superior processability. *Nat. Sci. Rev.* **2019**, nwz200. [[CrossRef](#)]
24. Cui, Y.; Yao, H.; Zhang, J.; Zhang, T.; Wang, Y.; Hong, L.; Xian, K.; Xu, B.; Zhang, S.; Peng, J.; et al. Over 16% efficiency organic photovoltaic cells enabled by a chlorinated acceptor with increased open-circuit voltages. *Nat. Commun.* **2019**, *10*, 2515. [[CrossRef](#)] [[PubMed](#)]

25. Fan, B.; Zhang, D.; Li, M.; Zhong, W.; Zeng, Z.; Ying, L.; Huang, F.; Cao, Y. Achieving over 16% efficiency for single-junction organic solar cells. *Sci. China Chem.* **2019**, *62*, 746–752. [[CrossRef](#)]
26. Doumon, N.Y.; Dryzhov, M.V.; Houard, F.V.; Le Corre, V.M.; Rahimi Chatri, A.; Christodoulis, P.; Koster, L.J.A. Photostability of fullerene and non-fullerene polymer solar cells: The role of the acceptor. *ACS Appl. Mater. Interfaces* **2019**, *11*, 8310–8318. [[CrossRef](#)]
27. Li, N.; McCulloch, I.; Brabec, C.J. Analyzing the efficiency, stability and cost potential for fullerene-free organic photovoltaics in one figure of merit. *Energy Environ. Sci.* **2018**, *11*, 1355–1361. [[CrossRef](#)]
28. Liu, Q.; Toudert, J.; Liu, F.; Mantilla-Perez, P.; Bajo, M.M.; Russell, T.P.; Martorell, J. Circumventing UV light induced nanomorphology disorder to achieve long lifetime PTB7-Th:PCBM based solar cells. *Adv. Energy Mater.* **2017**, *7*, 1701201. [[CrossRef](#)]
29. Lu, L.; Kelly, M.A.; You, W.; Yu, L. Status and prospects for ternary organic photovoltaics. *Nat. Phot.* **2015**, *9*, 491–500. [[CrossRef](#)]
30. Gupta, V.; Bharti, V.; Kumar, M.; Chand, S.; Heeger, A.J. Polymer-polymer Förster resonance energy transfer significantly boosts the power conversion efficiency of bulk-heterojunction solar cells. *Adv. Mater.* **2015**, *27*, 4398–4404. [[CrossRef](#)] [[PubMed](#)]
31. Felekidis, N.; Melianas, A.; Kemerink, M. Design rule for improved open-circuit voltage in binary and ternary organic solar cells. *ACS Appl. Mater. Interfaces* **2017**, *9*, 37070–37077. [[CrossRef](#)]
32. Gasparini, N.; Salleo, A.; McCulloch, I.; Baran, D. The role of the third component in ternary organic solar cells. *Nat. Rev. Mater.* **2019**, *4*, 229–242.
33. Lu, L.; Chen, W.; Xu, T.; Yu, L. High-performance ternary blend polymer solar cells involving both energy transfer and hole relay processes. *Nat. Comm.* **2015**, *6*, 7327. [[CrossRef](#)] [[PubMed](#)]
34. Liu, T.; Huo, L.; Sun, X.; Fan, B.; Cai, Y.; Kim, T. Ternary organic solar cells based on two highly efficient polymer donors with enhanced power conversion efficiency. *Adv. Energy Mater.* **2016**, *6*, 1502109. [[CrossRef](#)]
35. Gasparini, N.; Lucera, L.; Salvador, M.; Prosa, M.; Spyropoulos, G.D.; Kubis, P. High-performance ternary organic solar cells with thick active layer exceeding 11% efficiency. *Energy Environ. Sci.* **2017**, *10*, 885–892. [[CrossRef](#)]
36. Cha, H.; Chung, D.S.; Bae, S.Y.; Lee, M.J.; An, T.K.; Hwang, J. Complementary absorbing star-shaped small molecules for the preparation of ternary cascade energy structures in organic photovoltaic cells. *Adv. Funct. Mater.* **2013**, *23*, 1556–1565. [[CrossRef](#)]
37. Zhang, Y.; Deng, D.; Lu, K.; Zhang, J.; Xia, B.; Zhao, Y. Synergistic effect of polymer and small molecules for high-performance ternary organic solar cells. *Adv. Mater.* **2015**, *27*, 1071–1076. [[CrossRef](#)]
38. Zhang, S.; Zuo, L.; Chen, J.; Zhang, Z.; Mai, J.; Lau, T.K. Improved photon-to-electron response of ternary blend organic solar cells with a low band gap polymer sensitizer and interfacial modification. *J. Mater. Chem. A* **2016**, *4*, 1702–1707. [[CrossRef](#)]
39. Nian, L.; Gao, K.; Liu, F.; Kan, Y.; Jiang, X.; Liu, L. 11% efficient ternary organic solar cells with high composition tolerance via integrated near-IR sensitization and interface engineering. *Adv. Mater.* **2016**, *28*, 8184–8190. [[CrossRef](#)]
40. Zhang, J.; Zhao, Y.; Fang, J.; Yuan, L.; Xia, B.; Wang, G. Enhancing performance of large-area organic solar cells with thick film via ternary strategy. *Small* **2017**, *13*, 1700388. [[CrossRef](#)] [[PubMed](#)]
41. Zhang, G.; Zhang, K.; Yin, Q.; Jiang, X.F.; Wang, Z.; Xin, J. High-performance ternary organic solar cell enabled by a thick active layer containing a liquid crystalline small molecule donor. *J. Am. Chem. Soc.* **2017**, *139*, 2387–2395. [[CrossRef](#)] [[PubMed](#)]
42. Kai, Z.; Dandan, T.; Kaicheng, Z.; Zhaowei, W.; Lan, D.; Yanfeng, L.; Ligang, Y.; Jian, F.; Bo, S.; Zhou, Y.; et al. A two-dimension-conjugated small molecule for efficient ternary organic solar cells. *Org. Electron.* **2017**, *48*, 179–187. [[CrossRef](#)]
43. Wenzhan, X.; Chao, Y.; Xiang, Y.; Lili, J.; Xiong, G.; Yong, C. Efficient organic solar cells with polymer-small molecule: Fullerene ternary active layers. *ACS Omega* **2017**, *2*, 1786–1794. [[CrossRef](#)]
44. Pan, F.; Zhang, L.; Jiang, H.; Yuan, D.; Nian, Y.; Cao, Y.; Chen, J. As-cast ternary polymer solar cells based on a non-fullerene acceptor and its fluorinated counterpart showing improved efficiency and good thickness tolerance. *J. Mater. Chem. A* **2019**, *7*, 9798–9806. [[CrossRef](#)]
45. Rodríguez Seco, C.; Ferran, A.V.; Misra, R.; Sharma, G.D.; Palomares, E. Efficient non-polymeric heterojunctions in ternary organic solar cells. *ACS Appl. Energy Mater.* **2018**, *1*, 4203–4210. [[CrossRef](#)]

46. Mohapatra, A.A.; Kim, V.; Puttaraju, B.; Sadhanala, A.; Jiao, X.; McNeill, C.R.; Friend, R.H.; Patil, S. Förster resonance energy transfer drives higher efficiency in ternary blend organic solar cells. *ACS Appl. Energy Mater.* **2018**, *1*, 4874–4882. [[CrossRef](#)]
47. Ruiping, Q.; Guo, D.; Li, M.; Li, G.; Bo, Z.; Wu, J. Perylene monoimide dimers enhance ternary organic solar cells efficiency by induced D–A crystallinity. *ACS Appl. Energy Mater.* **2019**, *2*, 305–311. [[CrossRef](#)]
48. Fu, H.; Li, C.; Bi, P.; Hao, X.; Liu, F.; Li, Y.; Wang, Z.; Sun, Y. Efficient ternary organic solar cells enabled by the integration of nonfullerene and fullerene acceptors with a broad composition tolerance. *Adv. Funct. Mater.* **2019**, *29*, 1807006. [[CrossRef](#)]
49. Song, X.; Gasparini, N.; Nahid, M.M.; Harish, S.; Paleti, K.; Wang, J.L.; Ade, H.; Baran, D. Dual sensitizer and processing-aid behavior of donor enables efficient ternary organic solar cells. *Joule* **2019**, *3*, 1–12. [[CrossRef](#)]
50. Ke, L.; Gasparini, N.; Min, J.; Zhang, H.; Adam, M.; Rechberger, S. Panchromatic ternary/quaternary polymer/fullerene BHJ solar cells based on novel silicon naphthalocyanine and silicon phthalocyanine dye sensitizers. *J. Mater. Chem. A* **2017**, *5*, 2550–2562. [[CrossRef](#)]
51. Grant, T.M.; Gorisse, T.; Dautel, O.; Wantz, G.; Lessard, B.H. Multifunctional ternary additive in bulk heterojunction OPV: Increased device performance and stability. *J. Mater. Chem. A* **2017**, *5*, 1581–1587. [[CrossRef](#)]
52. Stylianakis, M.M.; Konios, D.; Viskadourous, G.; Vernardou, D.; Katsarakis, N.; Koudoumas, E.; Anastasiadis, S.H.; Stratakis, E.; Kymakis, E. Ternary organic solar cells incorporating zinc phthalocyanine with improved performance exceeding 8.5%. *Dyes Pigm.* **2017**, *146*, 408–413. [[CrossRef](#)]
53. Cheng, P.; Li, Y.; Zhan, X. Efficient ternary blend polymer solar cells with indene C₆₀ bis-adduct as an electron-cascade acceptor. *Energy Environ. Sci.* **2014**, *7*, 2005–2011. [[CrossRef](#)]
54. Sygletou, M.; Tzourmpakis, P.; Petridis, C.; Konios, D.; Fotakis, C.; Kymakis, E.; Stratakis, E. Laser induced nucleation of plasmonic nanoparticles on two-dimensional nanosheets for organic photovoltaics. *J. Mater. Chem. A* **2016**, *4*, 1020–1027. [[CrossRef](#)]
55. Bonaccorso, F.; Balis, N.; Stylianakis, M.M.; Savarese, M.; Adamo, C.; Gemmi, M.; Pellegrini, V.; Stratakis, E.; Kymakis, E. Functionalized graphene as an electron-cascade acceptor for air-processed organic ternary solar cells. *Adv. Funct. Mater.* **2015**, *25*, 3870–3880. [[CrossRef](#)]
56. Stylianakis, M.M.; Konios, D.; Kakavelakis, G.; Charalambidis, G.; Stratakis, E.; Coutsolelos, A.G.; Kymakis, E.; Anastasiadis, S.H. Efficient ternary organic photovoltaics incorporating a graphene-based porphyrin molecule as a universal electron cascade material. *Nanoscale* **2015**, *7*, 17827–17835. [[CrossRef](#)]
57. Stylianakis, M.M.; Konios, D.; Petridis, C.; Kakavelakis, G.; Stratakis, E.; Kymakis, E. Ternary solution-processed organic solar cells incorporating 2D materials. *2D Mater.* **2017**, *4*, 042005. [[CrossRef](#)]
58. Kakavelakis, G.; Esau, A.; Del Rio, C.; Pellegrini, V.; Ansaldo, A.; Tzourmpakis, P.; Brescia, R.; Prato, M.; Stratakis, E.; Kymakis, E.; et al. Size-tuning of WSe₂ flakes for high efficiency inverted organic solar cells. *ACS Nano* **2017**, *11*, 3517–3531. [[CrossRef](#)]
59. Stylianakis, M.M.; Kosmidis, D.M.; Anagnostou, K.; Polyzoidis, C.; Krassas, M.; Kenanakis, G.; Viskadourous, G.; Kornilios, N.; Petridis, K.; Kymakis, E. Emphasizing the operational role of a novel graphene-based ink into high performance ternary organic solar cells. *Nanomaterials* **2020**, *10*, 89. [[CrossRef](#)]
60. Balis, N.; Konios, D.; Stratakis, E.; Kymakis, E. Ternary organic solar cells with reduced graphene oxide–Sb₂S₃ hybrid nanosheets as the cascade material. *ChemNanoMat* **2015**, *1*, 5346–5352. [[CrossRef](#)]
61. Kozycz, L.M.; Gao, D.; Hollinger, J.; Seferos, D.S. Donor–donor block copolymers for ternary organic solar cells. *Macromolecules* **2012**, *45*, 5823–5832. [[CrossRef](#)]
62. You, J.; Dou, L.; Hong, Z.; Li, G.; Yang, Y. Recent trends in polymer tandem solar cells research. *Prog. Polym. Sci.* **2013**, *38*, 1909–1928. [[CrossRef](#)]
63. Yang, Y.M.; Chen, W.; Dou, L.; Chang, W.H.; Duan, H.S.; Bob, B. High-performance multiple-donor bulk heterojunction solar cells. *Nat. Photon.* **2015**, *9*, 190–198. [[CrossRef](#)]
64. Mancilha, F.S.; DaSilveira Neto, B.A.; Lopes, A.S.; Moreira, P.F.; Quina, F.H.; Gonçalves, R.S.; Dupont, J. Are molecular 5,8- π -extended quinoxaline derivatives good chromophores for photoluminescence applications? *Eur. J. Org. Chem.* **2006**, *2006*, 4924–4933. [[CrossRef](#)]
65. Yuan, J.; Zhang, Y.; Zhou, L.; Zhang, G.; Yip, H.L.; Lau, T.K.; Lu, X.; Zhu, C.; Peng, H.; Johnson, P.A.; et al. Single-junction organic solar cell with over 15% efficiency using fused-ring acceptor with electron-deficient core. *Joule* **2019**, *3*, 1140–1151. [[CrossRef](#)]

66. Akhtaruzzaman, M.; Tomura, M.; Nishida, J.; Yamashita, Y. New narrow-bandgap polymer composed of benzobis(1,2,5-thiadiazole) and thiophenes. *J. Am. Chem. Soc.* **1995**, *117*, 6791. [[CrossRef](#)]
67. Van Mullekom, H.A.; Vekemans, J.A.J.M.; Meijer, E.W. Band-gap engineering of donor–acceptor-substituted π -conjugated polymers. *Chem. Eur. J.* **1998**, *4*, 1235–1243. [[CrossRef](#)]
68. Park, S.H.; Roy, A.; Beaupre', S.; Cho, S.; Coates, N.; Moon, J.S.; Moses, D.; Leclerc, M.; Lee, K.; Heeger, A.J. Bulk heterojunction solar cells with internal quantum efficiency approaching 100%. *Nat. Photon.* **2009**, *3*, 297–302. [[CrossRef](#)]
69. Halls, J.J.M.; Walsh, C.A.; Greenham, N.C.; Marseglla, E.A.; Friend, R.H.; Moratti, S.C.; Holmes, A.B. Efficient photodiodes from interpenetrating polymer networks. *Nature* **1995**, *376*, 498–500. [[CrossRef](#)]
70. Mikroyannidis, J.A.; Stylianakis, M.M.; Dong, Q.; Zhou, Y.; Tian, W. New 4,7-dithienebenzothiadiazole derivatives with cyano-vinylene bonds: Synthesis, photophysics and photovoltaics. *Synth. Met.* **2009**, *159*, 1471–1477. [[CrossRef](#)]
71. Kraft, A.; Grimsdale, A.C.; Holmes, A.B. Electroluminescent conjugated polymers—Seeing polymers in a new light. *Angew. Chem. Int. Ed.* **1998**, *37*, 402–428. [[CrossRef](#)]
72. Cho, N.S.; Hwang, D.H.; Jung, B.J.; Oh, J.; Chu, H.Y.; Shim, H.K. Synthesis and light emitting properties of fluorene–carbazole-based conjugated copolymers. *Synth. Met.* **2004**, *143*, 277–282. [[CrossRef](#)]
73. Ochiai, S.; Imamura, S.; Kannappan, S.; Palanisamy, K.; Shin, P.K. Characteristics and the effect of additives on the nanomorphology of PTB7/PC₇₁BM composite films. *Cur. Appl. Phys.* **2013**, *13*, S58–S63. [[CrossRef](#)]
74. Konios, D.; Kakavelakis, G.; Petridis, C.; Savva, K.; Stratakis, E.; Kymakis, E. Highly efficient organic photovoltaic devices utilizing work-function tuned graphene oxide derivatives as the anode and cathode charge extraction layers. *J. Mater. Chem. A* **2016**, *4*, 1612–1623. [[CrossRef](#)]
75. Zhang, G.C.; Zhou, C.; Sun, C.; Jia, X.; Xu, B.; Ying, L.; Huang, F.; Cao, Y. An open-circuit voltage and power conversion efficiency study of fullerene ternary organic solar cells based on oligomer/oligomer and oligomer/polymer. *Macromol. Rapid Commun.* **2017**, *38*, 1700090. [[CrossRef](#)] [[PubMed](#)]
76. Campbell, A.J.; Bradley, D.D.C. Quantifying the efficiency of electrodes for positive carrier injection into poly(9,9-dioctylfluorene) and representative copolymers. *J. Appl. Phys.* **2001**, *89*, 3343. [[CrossRef](#)]
77. Kim, H.I.; Kim, M.; Park, C.W.; Kim, H.U.; Lee, H.-K.; Park, T. Morphological control of donor/acceptor interfaces in all-polymer solar cells using a pentafluorobenzene-based additive. *Chem. Mater.* **2017**, *29*, 6793–6798. [[CrossRef](#)]



© 2020 by the authors. Licensee MDPI, Basel, Switzerland. This article is an open access article distributed under the terms and conditions of the Creative Commons Attribution (CC BY) license (<http://creativecommons.org/licenses/by/4.0/>).